Available online at www.sciencedirect.com
ScienceDirect
Trans. Nonferrous Met. Soc. China 28(2018) 2265−2273
Transactions of Nonferrous Metals Society of China
www.tnmsc.cn

Preparation and catalytic behavior of reduced graphene oxide supported cobalt oxide hybrid nanocatalysts for CO oxidation

Yan WANG[1,4], Ze-hua CHEN[2], Jing HUANG[3], Gao-jie LI[2],
Jian-liang CAO[2], Bo ZHANG[2], Xing-ying CHEN[2], Huo-li ZHANG[2], Lei JIA[2]

1. College of Safety Science and Engineering, Henan Polytechnic University, Jiaozuo 454003, China;
2. College of Chemistry and Chemical Engineering, Henan Polytechnic University, Jiaozuo 454003, China;
3. Sinopec Research Institute of Petroleum Engineering,
China Petroleum Chemical Corporation, Beijing 100101, China;
4. Collaborative Innovation Center of Coal Work Safety of Henan Province, Jiaozuo 454003, China

Received 30 October 2016; accepted 6 June 2017

Abstract: The reduced graphene oxide (rGO) supported cobalt oxide nanocatalysts were prepared by the conventional precipitation and hydrothermal method. The as-prepared rGO−Co_3O_4 was characterized by the XRD, Raman spectrum, SEM, TEM, N_2-sorption, UV−Vis, XPS and H_2-TPR measurements. The results show that the spinel cobalt oxide nanoparticles are highly fragmented on the rGO support and possess uniform particle size, and the as-prepared catalysts possess high specific surface area and narrow pore size distribution. The catalytic properties of the as-prepared rGO−Co_3O_4 catalysts for CO oxidation were evaluated through a continuous-flow fixed-bed microreactor−gas chromatograph system. The catalyst with 30% (mass fraction) reduced graphene oxide exhibits the highest activity for CO complete oxidation at 100 °C.
Key words: reduced graphene oxide; cobalt oxide; catalyst; CO oxidation; catalytic activity

1 Introduction

Carbon monoxide (CO) is odorless, poisonous and fatal. Catalytic oxidation is the better removal method even for low concentration of CO. The oxidation of CO is one of the simplest and the most extensively investigated reactions in heterogeneous catalysis [1], so it has become one of the research focuses over the past years. At the same time, there is a growing need for highly efficient catalysts for low temperature CO oxidation. Up to now, many very effective noble metal catalysts such as Au [2], Pd [3,4], Pt [5,6] and Ru [7] have been developed for this reaction. However, the poor stability and high cost limit the applications of these noble metal catalysts. Thus, scientists continuously seek non-noble metal catalysts (Cu [8,9], Co [10,11], Mn [12]) in order to reduce the price and realize high efficient CO conversion. HU et al [10], JIA et al [11] and CAO et al [13] reported that cobalt oxide possesses almost the same catalytic activity to CO oxidation as the noble metal catalysts. The previous investigation [11] showed that the oxidant and surfactant were very important for obtaining the high catalytic activity cobalt oxide catalyst. However, the addition of the oxidant and surfactant may also cause the second pollution, the complicated process of preparation and the high cost. In addition, the nanostructured cobalt oxides are ready to aggregate due to the high surface energy, which may also lead to the degradation of catalytic activity. The preparation of supported catalysts can solve the above problem. At the same time, the supported catalysts can show a synergistic effect to induce properties that are different from those of each individual component.

Foundation item: Projects (51404097, 51504083, 21404033) supported by the National Natural Science Foundation of China; Project (2016M592290) supported by China Postdoctoral Science Foundation; Project (NSFRF1606) supported by the Fundamental Research Funds for the Universities of Henan Province, China; Projects (J2016-2, J2017-3) supported by Foundation for Distinguished Young Scientists of Henan Polytechnic University, China; Project (16A150009) supported by the Key Scientific Research Project for Higher Education of Henan Province, China; Project (166115) supported by the Postdoctoral Science Foundation of Henan Province, China; Project (17HASTIT029) supported by Program for Science & Technology Innovation Talents in Universities of Henan Province, China; Projects (162300410113, 162300410119) supported by Natural Science Foundation of Henan Province of China
Corresponding author: Ze-hua CHEN; Tel/Fax: +86-391-3987440; E-mail: chenzh2016@126.com
DOI: 10.1016/S1003-6326(18)64871-X

Due to the unique structure, intrinsic properties and easy surface modification, graphene has been regarded as one of the most excellent supports for various catalysts. Graphene-supported Pd [14], Pt [15], CeO_2 [16], TiO_2 [17] and MnO_2 [18] materials have been recently reported to possess high activities in many catalytic reactions. Theoretically, some studies have predicted that graphene-based catalysts maybe possess high activity for CO oxidation [19]. However, the research on catalytic application of graphene−Co_3O_4 hybrids for CO oxidation has been still rarely reported at present.

Therefore, in this work, we prepared a series of rGO−Co_3O_4 catalysts with different rGO contents by the hydrothermal method for CO oxidation, and further investigated the interaction between Co_3O_4 nanoparticles and reduced graphene oxide (rGO). The as-synthesized catalysts were characterized by various material characterization techniques. Catalytic CO oxidation activity tests were performed on a continuous-flow fixed-bed microreactor−gas chromatograph system.

2 Experimental

Natural graphite powder was purchased from Sinopharm Chemical Reagent Co., Ltd., with a mean particle size of 33 μm (99.85% purity). Graphite oxide was prepared from the natural graphite powder according to the method in Ref. [20]. Firstly, 1.5 graphite powders were added into 66 mL cold (0 °C) concentrated H_2SO_4 solution in a flask with three necks. Then, 1.5 g $NaNO_3$ and 9.0 g $KMnO_4$ were added gradually under stirring at a temperature below 4 °C, and then the mixture was continually stirred for 90 min. Secondly, the mixture was stirred at 35 °C for 30 min, and 132 mL distilled water was slowly added into the mixture at 70 °C. Thirdly, 30% H_2O_2 was added dropwise into the mixture solution until the color of mixture turned bright yellow. The solution was centrifugated and washed with 0.5 mol/L HCl solution and then deionized (DI) water to remove impurities. The precipitate was dispersed in a certain amount of DI water by sonication for 90 min to achieve uniform dispersion of graphene oxide (GO).

2.49 $Co(C_2H_3O_2)_2{\cdot}4H_2O$ was dispersed in 50 mL DI water and a calculated amount of GO (1.12%, GO in DI water) was added into 250 mL DI water under ultrasonic treatment for 20 min. Then, $Co(C_2H_3O_2)_2{\cdot}4H_2O$ solution was slowly added into the GO solution under magnetic stirring. Ammonia solution (26 mL, 28%) was added into the above solution for cobalt ion precipitation and GO reduction [21]. Finally, the mixture was transferred into a Teflon-lined stainless steel autoclave (500 mL) and heated at 180 °C for 12 h. The product was separated by centrifuging and washed several times with DI water and ethanol. The obtained composite was dried in air at 60 °C for 8 h and labeled as xrGO−Co_3O_4 (x=w(GO)/[w(GO)+w(Co_3O_4)×100%]. In order to remove the residual water and improve the crystallinity of the cobalt oxide, the prepared hybrids were heated at 160 °C for 4 h. For comparison, pure rGO and Co_3O_4 were prepared in the same way in the absence of $Co(C_2H_3O_2)_2{\cdot}4H_2O$ or graphene oxide.

X-ray diffraction (XRD) analysis was performed on a Bruker-AXS D8 advance diffractometer, with Cu K_α radiation at 40 kV and 25 mA. Raman spectra data were obtained by an inVia Reflex Raman microscope. The morphology of the as-prepared samples has been measured by using scanning electron microscope (SEM, JEOL JSM−6390LV). Transmission electron microscopy (TEM) analysis was performed on a JEOL JEM−2100 microscope, operating at 200 kV. N_2 adsorption−desorption isotherms were collected at liquid nitrogen temperature using a Quantachrome NOVA 2000e sorption analyzer, and the sample was degassed at 180 °C for 6 h. The specific surface areas of the samples were calculated following the multi-point BET procedure. The thermogravimetry−differential thermal analysis (TG−DTA) was conducted on a NETZSCH STA449C simultaneous thermal analyzer in air atmosphere (flow rate: 90 mL/min; heat rate: 10 °C/min). UV−Vis absorption spectroscopy measurements were carried out on a TU−1810 spectrometer. Hydrogen temperature-programmed reduction (H_2-TPR) analysis was performed under the mixture of 5% H_2 in N_2 flowing (30 mL/min) over 50 mg of catalyst at a heating rate of 10 °C/min from 0 to 800 °C. X-ray photoelectron spectroscopy (XPS) measurements were carried out on a Perkin-Elmer PHI 5600 spectrophotometer with Mg K_α radiation, and the C 1s peak was fixed at a binding energy of 284.6 eV.

CO oxidation activities of the as-prepared rGO−Co_3O_4 catalysts were tested on a continuous-flow fixed-bed microreactor−gas chromatograph system. The catalytic activity test method is the same as that of our previously published paper [22].

3 Results and discussion

3.1 Characterization of as-prepared samples

Figure 1(a) shows the XRD patters of GO and rGO. The absence of the most intensive peak of GO for rGO demonstrates the effective reduction of GO to rGO. Figure 1(b) shows the XRD patterns of rGO−Co_3O_4 hybrids with different rGO contents. The major diffraction peaks of all the samples are well indexed with space group $Fd\bar{3}m$ (227) (JCPDS No. 43−1003), implying the formation of single-phase spinel Co_3O_4. Compared with the pure Co_3O_4, no obvious diffraction peak (002) of graphene appears at 2θ of 23°−28°. This could be attributed to the disorderedly stacked and less

agglomeration of graphene sheets. The average sizes of the Co_3O_4 nanoparticles in the rGO−Co_3O_4 hybrids are 22.8, 17.1, 20.4, 22.3, 24.3 and 27.5 nm, respectively.

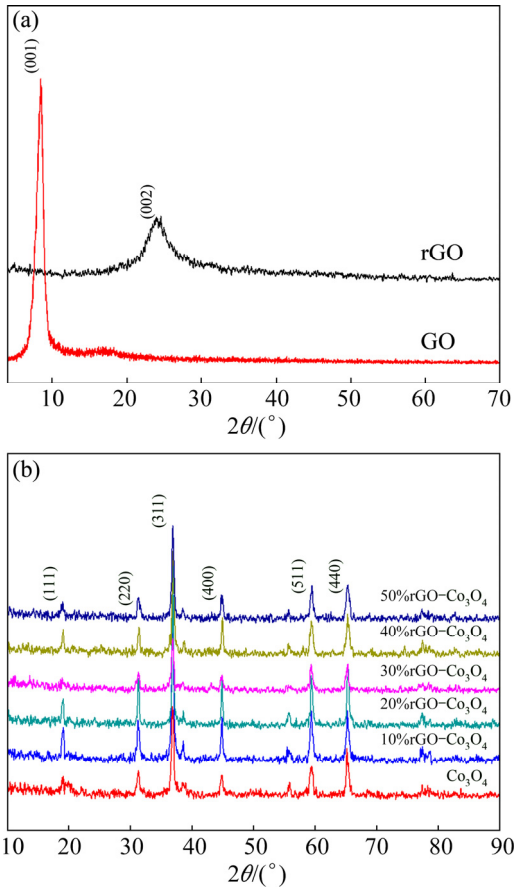

Fig. 1 XRD patterns of GO and rGO (a), and rGO−Co_3O_4 hybrid composites with different rGO contents (b)

The Raman spectra of GO, rGO, and rGO−Co_3O_4 hybrids with different rGO contents are shown in Fig. 2. In Fig. 2(a), the broad peaks displayed at 1351 and 1604 cm^{-1} could be assigned to the D and G peaks of graphene [23]. The D peak is the defect peak, which reflects the disorder of graphene sheets. In addition, the D band is prominent, indicating the reduction of the in-plane sp^2 domains. The G peak is the characteristic peak of sp^2-hybridized carbon, which reflects symmetry and crystallization of C sp^2 atoms. Compared with GO, an increased D/G intensity ratio in rGO suggests a decrease in the average size of the sp^2 domains upon reduction [24]. The Raman spectra of the rGO−Co_3O_4 hybrids with different rGO contents (Fig. 2(b)) demonstrate the existence of graphene. In addition, the peaks at around 188, 505 and 592 cm^{-1} could be attributed to the F_{2g} mode of Co_3O_4, and the peaks at 469 and 665 cm^{-1} are ascribed to the E_g and A_{1g} modes of Co_3O_4, respectively [21,25].

Figures 3(a) and (b) reveal the general structure of the 30%rGO−Co_3O_4 hybrid composite. As shown in Fig. 3(a), the graphene layers are exfoliated to a large extent. The porous structure with very thin planes indicates that the overall structure is dominated by the graphene network. Moreover, the structure of the rGO support can prevent the aggregation of the Co_3O_4 nanoparticles which can increase the effective surface area. From Figs. 3(b) and (c), the Co_3O_4 nanoparticles with size about 20 nm are uniformly distributed on the graphene plane.

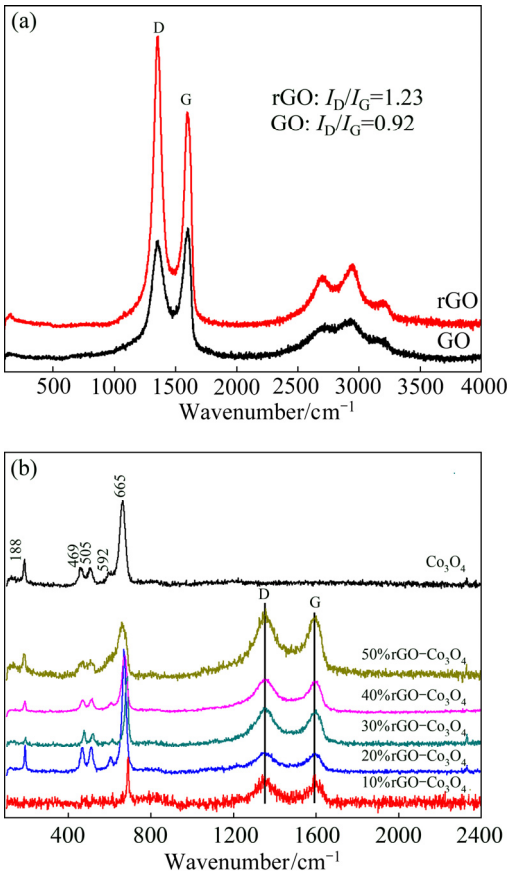

Fig. 2 Raman spectra of GO and rGO (a), and rGO−Co_3O_4 hybrid composites with different rGO contents (b)

Figure 4(a) shows that the rGO substrate is almost transparent. Figure 4(b) shows the lattice image clearly. The spaces between the lattice fringes which are consistent with (111) and (220) planes of Co_3O_4 are about 0.46 and 0.285 nm, respectively. Selected-area electron diffraction (SAED) image in this region confirms the pattern of Co_3O_4. In addition, the average particle size of cobalt oxide is determined to be about 20 nm.

The N_2-sorption analysis results of the rGO, 30%rGO−Co_3O_4, and the 40%rGO−Co_3O_4 hybrid composites are shown in Fig. 5. The textural properties are listed in Table 1. The isotherms of these three samples (Fig. 5(a)) are of type IV, characteristic of mesoporous materials. All of these samples show well-defined hysteresis loop of type H3, indicating the

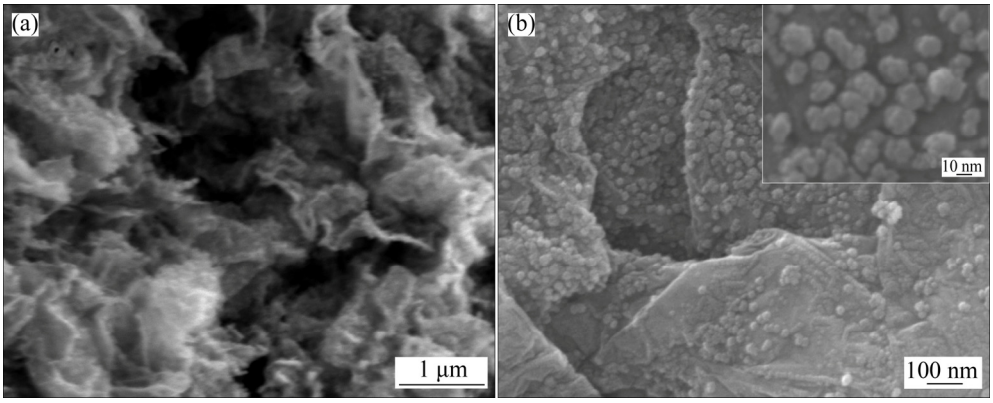

Fig. 3 Lower (a) and higher (b) magnified SEM images of 30%rGO−Co_3O_4 hybrid composite

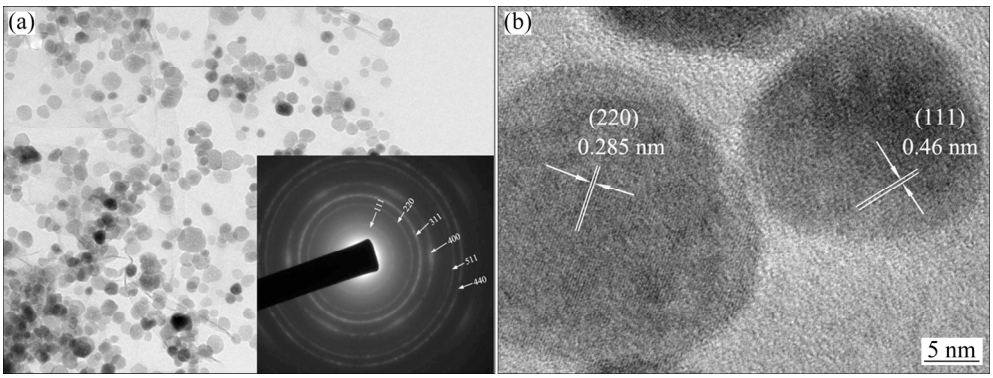

Fig. 4 TEM (a) and HRTEM (b) images of 30%rGO−Co_3O_4 hybrid composite

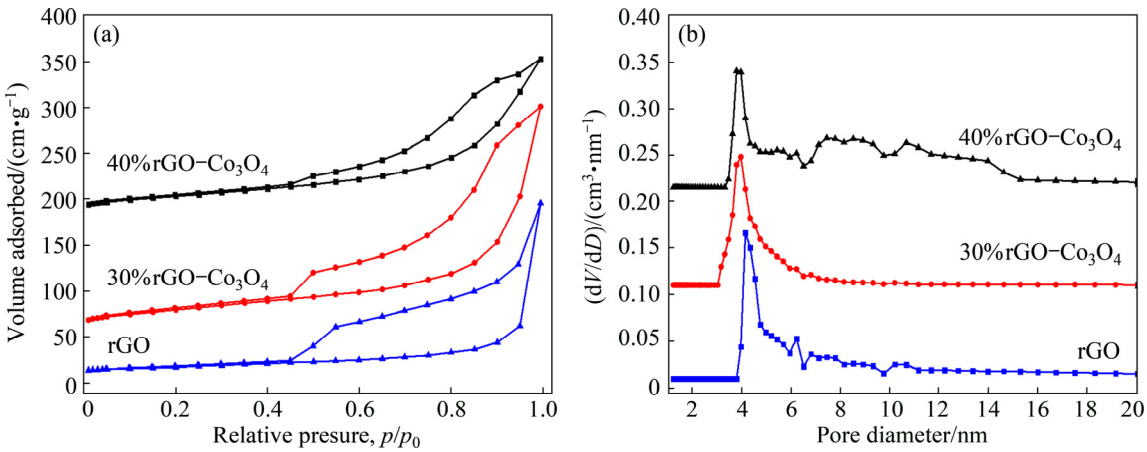

Fig. 5 N_2 adsorption−desorption isotherms (a) and corresponding pore size distribution curves (b) of as-prepared samples of rGO, 30%rGO−Co_3O_4, and 40%rGO−Co_3O_4 (Volumes were shifted by 50 and 180 cm^3/g for curves of 30%rGO−Co_3O_4 and 40%rGO−Co_3O_4 samples, and dV/dD values were shifted by 0.11 and 0.21 $cm^3/(g·nm)$ for curves of 30%rGO−Co_3O_4 and 40%rGO−Co_3O_4, respectively)

Table 1 Textural properties and catalytic activities of investigated catalysts

Sample	Surface area[a]/($m^2·g^{-1}$)	Pore volume[b]/($cm^3·g^{-1}$)	$D_{DFT\text{-}ads}$[c]/nm	T_{50}[d]/°C	T_{100}[e]/°C
rGO	127	0.28	3.82	240	280
30%rGO−Co_3O_4	202	0.24	3.82	82	100
40%rGO−Co_3O_4	195	0.43	3.81	92	110

[a] Multi-point BET surface area; [b] Total pore volume at p/p_0=0.994; [c] Maximum of DFT pore diameter as determined from adsorption branch; [d] Temperature when conversion of CO is 50%; [e] Temperature when conversion of CO is 100%

disorderedly stacked graphene nanosheets and the presence of slit-like pores. The pore size distributions were determined by the DFT methods from the adsorption branch of the isotherms. In Fig. 5(b), the samples exhibit quite narrow pore size distribution peaks. This porosity should come from the organized aggregation of Co_3O_4 nanoparticles. It is noted from Fig. 5(b) that the adsorption isotherm of the sample exhibits a large increase at the p/p_0 above 0.9. This proves the presence of the secondary large pores (macropores) [26]. The specific surface area of rGO is 127 m^2/g, less than the theoretical value of graphene, which may be caused by serious aggregation of graphene sheets. Compared with that of rGO, the specific surface area of the hybrid composites has a significant increase, which could be ascribed to the introduction of Co_3O_4 nanoparticles.

Figure 6 shows the representative TG−DTA curves of the 30%rGO−Co_3O_4 hybrid nanocomposite. The process of mass loss can be divided into three steps. The endothermic peak between 40 and 130 °C on DTA curve, accompanied by 3% of mass loss on TG curve, is assigned to the physical or chemical adsorption on the interparticle surface of the sample. The second stage from 130 to 400 °C with 5% mass loss might correspond to the decomposition of oxygen functional groups of the graphene. It is noted that the decomposition temperature of the sample ranges from 400 to 700 °C with a main mass loss of about 29%, accompanied with a strong exothermic peak around 607 °C. This is attributed to the decomposition and combustion of carbon skeleton [27]. The total mass loss is 37%. No crystalline phase transformation is observed. The result of TG−DTA demonstrates that the as-prepared catalysts are very stable at 400 °C.

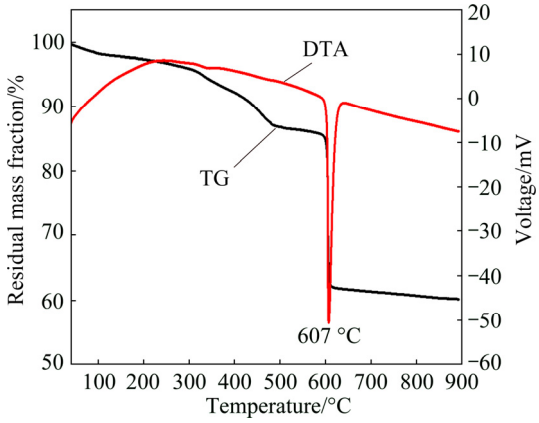

Fig. 6 TG−DTA curves of 30%rGO−Co_3O_4 hybrid composite

The UV−Vis spectra of pure Co_3O_4 and the rGO−Co_3O_4 hybrids are shown in Fig. 7. As shown in Fig. 7, two absorption bands centered at 270 and 450 nm correspond to the two band gaps of the sample. In the previous investigation [28], the first band gaps can be assigned to the ligand-to-metal charge transfer from O^{2-} to Co^{2+} (basic optical band gap energy, or valence to conduction band excitation). The second band gap can be assigned to charge transfer from O^{2-} to Co^{3+} (Co^{3+} level located below the conduction band). Compared with that of the pure Co_3O_4, the absorption edges of all the rGO−Co_3O_4 hybrid composites shift to lower energy. Increasing the content of rGO, the red shift of absorption edge for the rGO−Co_3O_4 hybrid composites becomes more obvious. Hence, the introduction of graphene fades the band energy of Co—O bond and causes the extraction of lattice oxygen easier from the surface of Co_3O_4.

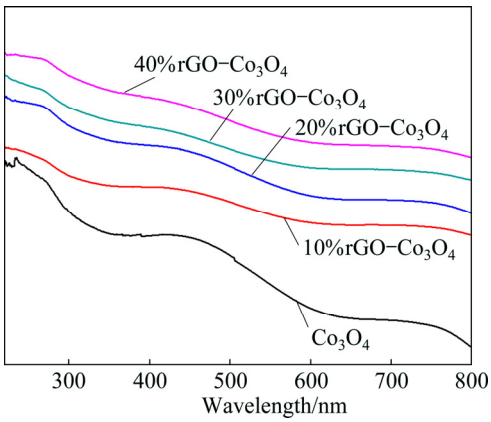

Fig. 7 UV−Vis spectra of Co_3O_4 and rGO−Co_3O_4 hybrid composites with different rGO contents

Figure 8 shows the H_2-TPR profiles of the 30%rGO−Co_3O_4 hybrid composite. The reduction profiles of the pure Co_3O_4 and the rGO powders are also presented. For the pure Co_3O_4, two obvious reduction peaks centered at 355 and 495 °C are detected, which can be ascribed to the reduction of Co^{3+} to Co^{2+} and Co^{2+} to Co^0 [10], respectively. For the rGO support, a large reduction peak appeared in the temperature range of 400−800 °C.

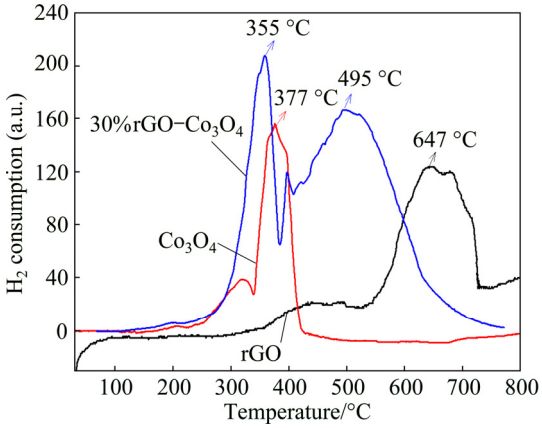

Fig. 8 H_2-TPR profiles of Co_3O_4, rGO, and 30%rGO−Co_3O_4 hybrid composite

In the H_2-TPR profile of the 30%rGO−Co_3O_4 hybrid composite, the reduction peak of rGO shifts to the lower temperature. This reveals that the Co_3O_4 can lower the reduction temperature of the rGO. The main temperature reduction peak of the rGO−Co_3O_4 sample is also much lower than that of the pure Co_3O_4. There is a synergistic effect between Co_3O_4 and rGO.

XPS analysis was performed to understand the valence states of the elements present in the 30%rGO−Co_3O_4 hybrid composite. Figure 9(a) shows the general survey spectrum. It reveals that the surface of the hybrid composite contains Co, C and O elements. The Co 2p XPS spectrum of the composite shows two peaks at 780.4 and 795.6 eV, corresponding to the Co $2p^{1/2}$ and Co $2p^{3/2}$ spin-orbit peaks of Co_3O_4 (Fig. 9(b)) [29]. Four peaks at 284.7, 286.1, 287.5 and 289.1 eV correspond to C—C (C sp^2), C—OH, C—O—C and O═C—OH groups, respectively (Fig. 9(c)) [3]. Compared with the sp^2 C—C peak, the peak of oxygen functional groups is weaker, which illustrates the almost complete reduction of GO [30]. The XPS spectrum of O 1s (Fig. 9(d)) shows a main peak centered at 530.08 eV and a broad shoulder at about 531.48 eV, which illustrate the existence of two different oxygen species. This indicates that the first peak in the range of 529.7−530.7 eV is the "O^{2-}" ions of the lattice oxygen, and the second peak in the range of 531.0−532.0 eV is attributed to the chemisorbed oxygen.

3.2 Catalytic activity

Figure 10 shows the catalytic activities for CO oxidation of the Co_3O_4, rGO and rGO−Co_3O_4 hybrid catalysts with different contents of rGO in the temperature range of 50−150 °C. As shown in Fig. 10, with the increase of the catalytic reaction temperature, the conversion rate of CO increased, while the pure rGO support has no activity. Besides, the sharp peak close to T_{100} (the temperature at CO conversion rate of 100%) can be attributed to the fact that O_2 molecule gets enough energy. The total oxidation temperature of CO (T_{100}) can be achieved at 100, 110, 130, 100, 140 and 130 °C, over the rGO−Co_3O_4 hybrid catalysts with the rGO contents of 0, 10%, 20%, 30%, 40%, and 50%, respectively. The 30%rGO−Co_3O_4 hybrid catalyst possesses the same catalytic activity of the pure Co_3O_4. However, in order to compare the activity between the pure Co_3O_4 and the rGO−Co_3O_4, the amounts of the CO converted per gram of the Co_3O_4 in unit time have been calculated, which are 2.2 and 3.14 L/h for the pure Co_3O_4 and the 30%rGO−Co_3O_4 hybrid, respectively. This reduced graphene oxide supported Co_3O_4 hybrid nanocatalyst shows much higher catalytic activity than the previous

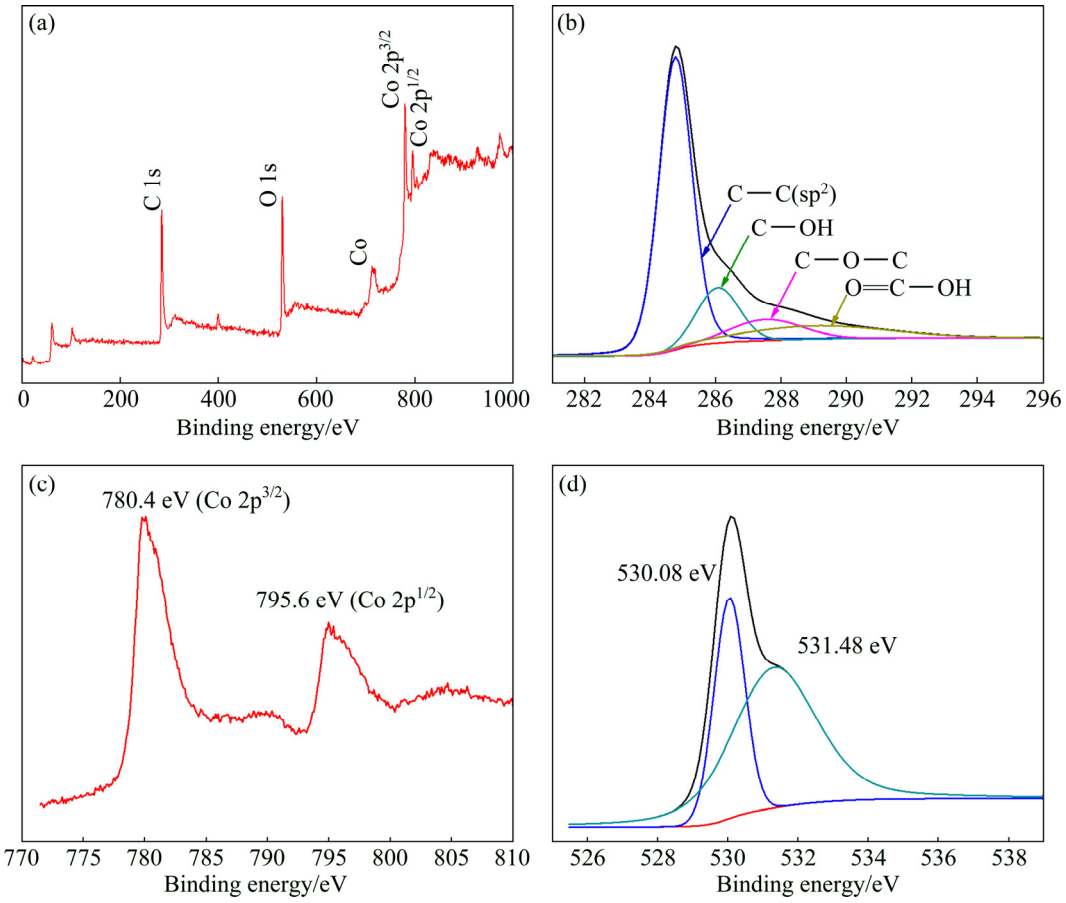

Fig. 9 XPS analysis of 30%rGO−Co_3O_4 sample: (a) General scan of 30%rGO−Co_3O_4 sample; (b) C 1s; (c) Co 2p; (d) O 1s

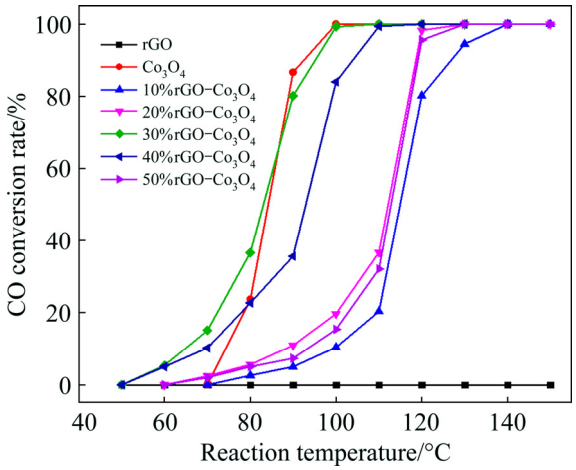

Fig. 10 Catalytic activity for CO oxidation of pure Co_3O_4, rGO, and rGO−Co_3O_4 hybrid catalysts with different rGO contents

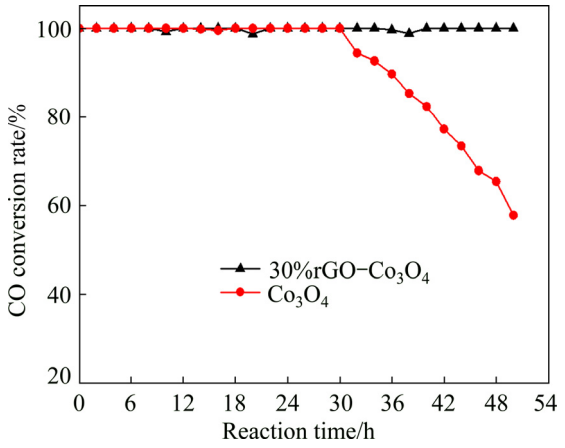

Fig. 11 CO conversion rates of Co_3O_4 and 30%rGO−Co_3O_4 hybrid catalysts at 100 °C as function of reaction time

reported CeO_2 (T_{100}=147 °C [31], T_{100}=150 °C [32], T_{50}=135 °C [33], T_{50}=94 °C [34]), SiO_2 (T_{100}=170 °C), TiO_2 (T_{100}=270 °C), Al_2O_3 (T_{100}=220 °C) [35] and the mesoporous Co—Fe—O nanocatalysts (T_{100}= 140 °C) [13,36].

In addition, the rGO−Co_3O_4 composite catalysts reveal good stability at 100 °C, as shown in Fig. 11. For the pure Co_3O_4, the conversion rate of CO keeps at 100% steadily for 30 h at 100 °C. The conversion rate of CO drops rapidly after 30 h, and becomes lower than 60% after 48 h reaction. This is due to the aggregation of the Co_3O_4 nanoparticles and the consumption of active oxygen on the surface of Co_3O_4 nanoparticles. For the 30%rGO−Co_3O_4 hybrid catalyst, the CO conversion rate can maintain at 100% during the testing time at 100 °C. The high specific surface area and excellent electronic transmission performance create the high stability. As reported in the literature, some other catalysts also showed the similar stability, such as Pd/graphene [3] and Au/TiO_2 [37].

Many studies about CO oxidation reaction mechanism on the surface of Co_3O_4 nanoparticles have been reported. However, there is no consistent conclusion report until now. Most researchers believe that Co^{3+} is the active site of adsorbing CO and surface lattice oxygen is directly involved in the course of oxidation−reduction process [38,39]. In this study, we proposed a potential pathway for CO oxidation of rGO−Co_3O_4 hybrid composite catalysts, as shown in Fig. 12. Firstly, O_2 molecular is dissociated into reactive oxygen species. Secondly, CO is adsorbed on the surface as bidentate carbonate. The TPR and UV−Vis results have confirmed that the Co—O bond of the as-prepared composites breaks up more easily than that of the pure Co_3O_4. It can also explain indirectly the phenomenon that the as-prepared composite is better than the pure Co_3O_4 in CO conversion at low temperature. Thirdly, the first potential pathway is that the adsorbed CO reacts with active oxygen to form CO_2 on the surface of Co_3O_4 nanoparticles. The second potential pathway is that the adsorbed CO extracts surface lattice oxygen of Co_3O_4 nanoparticles to form CO_2 and surface oxygen vacancy. The CO_2 molecular breaks away from the surface of the Co_3O_4 nanoparticles and the vacancy is filled by gas phase O_2. It is considered to be present possibly as O_2^- ion radical [40], and may combine with the neighboring CO molecule adsorbed as bidentate carbonate, forming CO_2 again and recovering from the catalyst surface. The third potential pathway is that the oxygen vacancy is filled by the active oxygen species transferred by the reduced graphene oxide support.

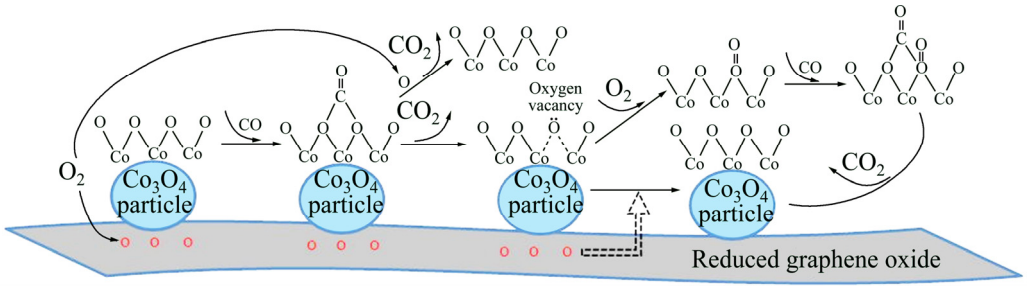

Fig. 12 Proposed reaction pathway for CO oxidation in the presence of as-obtained rGO−Co_3O_4 hybrid catalyst

4 Conclusions

1) Reduced graphene oxide supported Co_3O_4 hybrid nanocatalysts are successfully prepared via a simple hydrothermal method. SEM and TEM images show that the Co_3O_4 nanoparticles are uniformly distributed on the graphene plane. The size of Co_3O_4 nanoparticles is about 20 nm.

2) The rGO−Co_3O_4 hybrid catalysts show high activity and stability for CO oxidation. The enhanced stability can be ascribed to the graphene substrates. The graphene substrates can prevent the aggregation of Co_3O_4 nanoparticles and provide more active sites. The conversion rate of CO has been further improved at low temperature. This is mainly due to the fact that graphene can weaken the band energy of Co—O bond and make the extraction of lattice oxygen easier from the surface of Co_3O_4. The present study is helpful for the design of graphene support transition metal catalysts with high efficiency and stability for CO oxidation.

References

[1] HARUTA M, TSUBOTA S, KOBAYASHI T. Low-temperature oxidation of CO over gold supported on TiO_2, α-Fe_2O_3, and Co_3O_4 [J]. Journal of Catalysis, 1993, 144(1): 175−192.

[2] AVGOUROPOULOS G, MANZOLI M, BOCCUZZI F. Catalytic performance and characterization of Au/doped-ceria catalysts for the preferential CO oxidation reaction [J]. Journal of Catalysis, 2008, 256(2): 237−247.

[3] LI Ying-zhi, YU Yue, WANG Jian-guo, SONG Jie, LI Qiang, DONG Ming-dong, LIU Chang-jun. CO oxidation over graphene supported palladium catalyst [J]. Applied Catalysis B, 2012, 125: 189−196.

[4] CHEN Shu-tang, SI Rui, TAYLOR E, JANZEN J, CHEN Jing-yi. Synthesis of Pd/Fe_3O_4 hybrid nanocatalysts with controllable interface and enhanced catalytic activities for CO oxidation [J]. The Journal of Physical Chemistry C, 2012, 116(23): 12969−12976.

[5] ENGEL T, ERTL G. Elementary steps in the catalytic oxidation of carbon monoxide on platinum metals [J]. Advances in Catalysis, 1979, 28: 1−78.

[6] CHUA Y P G, GUNASOORIYA G T K K. Controlling the CO oxidation rate over Pt/TiO_2 catalysts by defect engineering of the TiO_2 support [J]. Journal of Catalysis, 2014, 311: 306−313.

[7] CHEN H T. First-principles study of CO adsorption and oxidation on Ru-doped CeO_2 (111) surface [J]. The Journal of Physical Chemistry C, 2012, 116(10): 6239−6246.

[8] CAO Jian-liang, WANG Yan, YU Xiu-ling, WANG Shu-rong, WU Shi-hua, YUAN Zhong-yong. Mesoporous CuO−Fe_2O_3 composite catalysts for low-temperature carbon monoxide oxidation [J]. Applied Catalysis B, 2008, 79(1): 26−34.

[9] LUO Meng-fei, MA Jing-meng, LU Ji-qing, SONG Yu-peng, WANG Yue-juan. High-surface area CuO−CeO_2 catalysts prepared by a surfactant-templated method for low-temperature CO oxidation [J]. Journal of Catalysis, 2007, 246(1): 52−59.

[10] HU Lin-hua, SUN Ke-qiang, PENG Qing, XU Bo-qing, LI Ya-dong. Surface active sites on Co_3O_4 nanobelt and nanocube model catalysts for CO oxidation [J]. Nano Research, 2010, 3(5): 363−368.

[11] JIA Ming-jun, ZHANG Wen-xiang, TAO Yu-guo, WANG Gui-ying, CUI Xiang-hao, ZHANG Chun-lei, WU Tong-hao, DONG Guo-qiang. Preparation, characterization and CO oxidation of nanometer Co_3O_4 [J]. Chemical Research in Chinese University, 1999, 4: 637−639.

[12] XIAO Jun-wu, WAN Lian, WANG Xue, KUANG Qin, DONG Shuang, XIAO Fei, WANG Shuai. Mesoporous Mn_3O_4–CoO core–shell spheres wrapped by carbon nanotubes: A high performance catalyst for the oxygen reduction reaction and CO oxidation [J]. Journal of Materials Chemistry A, 2014, 2: 3794−3800.

[13] CAO Jian-liang, YAN Zhao-li, WANG Yan, SUN Guang, WANG Xiao-dong, BALA Hari, ZHANG Zhan-ying. CTAB-assisted synthesis of mesoporous $CoFe_2O_4$ with high carbon monoxide oxidation activity [J]. Materials Letters, 2013, 106: 322−325.

[14] ZHANG Yan, WANG Qin, YE Wei-chun, LI Jia-jia, WANG Chun-ming. Pd micro-nanoparticles electrodeposited on graphene/ polyimide membrane for electrocatalytic oxidation of formic acid [J]. Transactions of Nonferrous Metals Society of China, 2015, 25(9): 2986−2993.

[15] YOO E J, OKATA T, AKITA T, KOHYAMA M, NAKAMURA J, HONMA I. Enhanced electrocatalytic activity of Pt subnanoclusters on graphene nanosheet surface [J]. Nano Letters, 2009, 9: 2255−2259.

[16] WANG Yi, GUO Chun-xian, LIU Jie-hua, CHEN Tao, YANG Hong-bin, LI Chang-ming. CeO_2 nanoparticles/graphene nano-composite-based high performance supercapacitor [J]. Dalton Transactions, 2011, 40: 6388−6391.

[17] PERERA S D, MARIANO R G, VU K, NOUR N, SEITZ O, CHABAL Y, BALKUS K J. Hydrothermal synthesis of graphene−TiO_2 nanotube composites with enhanced photocatalytic activity [J]. ACS Catalysis, 2012, 2(6): 949−956.

[18] HE Yong-min, CHEN Wan-jun, LI Xiao-dong, ZHANG Zhen-xing, FU Jie-cai, ZHAO Chang-hui, XIE Er-qing. Freestanding three-dimensional graphene/MnO_2 composite networks as ultralight and flexible supercapacitor electrodes [J]. ACS Nano, 2013, 7(1): 174−182.

[19] LI Feng-yu, ZHAO Ji-jun, CHEN Zhong-fang. Fe-anchored graphene oxide: A low-cost and easily accessible catalyst for low-temperature CO oxidation [J]. The Journal of Physical Chemistry C, 2012, 116(3): 2507−2514.

[20] HUMMERS W S, OFFEMAN R E. Preparation of graphitic oxide [J]. Journal of the American Chemical Society, 1958, 80(6): 1339−1339.

[21] KIM H, SEO D H, KIM S W, KIM J, KANG K. Highly reversible Co_3O_4/graphene hybrid anode for lithium rechargeable batteries [J]. Carbon, 2011, 49(1): 326−332.

[22] CAO Jian-liang, LI Gao-jie, WANG Yan. Oil shale ash supported CuO nanocatalysts: Preparation, characterization and catalytic activity for CO oxidation [J]. Journal of Environmental Chemical Engineering, 2015, 3(3): 1725−1730.

[23] PARK S, AN J H, PINER R D, JUNG I, YANG D X, VELAMAKANNI A, NGUYEN S T, RUOFF R S. Aqueous suspension and characterization of chemically modified graphene sheets [J]. Chemistry of Materials, 2008, 20(21): 6592−6594.

[24] TUINSTRA F, KOENIG J L. Raman spectrum of graphite [J]. The Journal of Physical Chemistry C, 1970, 53: 1126−1130.

[25] JIANG Jing, LI Liang-chao. Synthesis of sphere-like Co_3O_4 nanocrystals via a simple polyol route [J]. Materials Letters, 2007, 61(27): 4894−4896.

[26] YUAN Zhong-yong, REN Tie-zhen, VANTOMME A, SU Bao-lian. Facile and generalized preparation of hierarchically mesoporous-macroporous binary metal oxide materials [J]. Chemistry of Materials, 2004, 16(24): 5096−5106.

[27] YAO Yun-jin, YANG Ze-heng, SUN Hong-qi, WANG Shao-bin. Hydrothermal synthesis of Co_3O_4−graphene for heterogeneous activation of peroxymonosulfate for decomposition of phenol [J]. Industrial & Engineering Chemistry Research, 2012, 51(46): 14958−14965.

[28] LOU Y, MA J, CAO X M, WANG L, DAI Q G, ZHAO Z Y, CAI Y F, ZHAN W C, GUO Y L, HU P, LU G Z, GUO Y. Promoting effects of In_2O_3 on Co_3O_4 for CO oxidation: Tuning O_2 activation and CO Adsorption Strength Simultaneously [J]. ACS Catalysis, 2014, 4(11): 4143−4152.

[29] WU Zhong-shuai, REN Wen-cai, WEN Lei, GAO Li-bo, ZHAO Jin-ping, CHEN Zong-ping, ZHOU Guang-min, LI Feng, CHENG Hui-ming. Graphene anchored with Co_3O_4 nanoparticles as anode of lithium ion batteries with enhanced reversible capacity and cyclic performance [J]. ACS Nano, 2010, 4(6): 3187−3194.

[30] GAO Li-na, YUE Wen-bo, TAO Shan-shan, FAN Lou-zhen. Novel strategy for preparation of graphene−Pd, Pt composite, and its enhanced electrocatalytic activity for alcohol oxidation [J]. Langmuir, 2013, 29(3): 957−964.

[31] KANG M, SONG M W, KIM K L. Catalytic oxidation of carbon monoxide over CoO_x/CeO_2 catalysts [J]. Reaction Kinetics, Mechanisms and Catalysis, 2003, 79(1): 3−10.

[32] TANG C W, KUO M C, LIN C J, WANG C B, CHIEN S H. Evaluation of carbon monoxide oxidation over CeO_2/Co_3O_4 catalysts: Effect of ceria loading [J]. Catalysis Today, 2008, 131: 520−525.

[33] KANG M, SONG M W, LEE C H. Catalytic carbon monoxide oxidation over CoO_x/CeO_2 composite catalysts [J]. Applied Catalysis A, 2003, 251: 143−156.

[34] LUO Jin-yong, MENG Ming, LI Xiang, LI Xin-gang, ZHA Yu-qing, HU Tian-dou, XIE Ya-ning, ZHANG Jing. Mesoporous Co_3O_4−CeO_2 and Pd/Co_3O_4−CeO_2 catalysts: Synthesis, characterization and mechanistic study of their catalytic properties for low-temperature CO oxidation [J]. Journal of Catalysis, 2008, 254(2): 310−324.

[35] WANG C B, TANG C W, TSAI H C, CHIEN S H. Characterization and catalytic oxidation of carbon monoxide over supported cobalt catalysts [J]. Catalysis Letters, 2006, 107(3−4): 223−230.

[36] CAO Jian-liang, LI Gao-jie, WANG Yan, SUN Guang, WANG Xiao-dong, HARI Bala, ZHANG Zhan-ying. Mesoporous Co−Fe−O nanocatalysts: Preparation, characterization and catalytic carbon monoxide oxidation [J]. Journal of Environmental Chemical Engineering, 2014, 2: 477−483.

[37] SCHUMACHER B, PLZAK V, KINNE M, BEHM R J. Highly active Au/TiO_2 catalysts for low-temperature CO oxidation: Preparation, conditioning and stability [J]. Catalysis Letters, 2003, 89(1−2): 109−114.

[38] BROQVIST P, PANAS I, PERSSON H. A DFT study on CO oxidation over Co_3O_4 [J]. Journal of Catalysis, 2002, 201(2): 198−206.

[39] POLLARD M J, WEINSTOCK B A, BITTERWOLF T E, GRIFFITHS P R, NEWBERY A P, PAINE J B. A mechanistic study of the low-temperature conversion of carbon monoxide to carbon dioxide over a cobalt oxide catalyst [J]. Journal of Catalysis, 2008, 254(2): 218−225.

[40] SEDMAK G, HOČEVAR S, LEVEC J. Kinetics of selective CO oxidation in excess of H_2 over the nanostructured $Cu_{0.1}Ce_{0.9}O_{2-y}$ catalyst [J]. Journal of Catalysis, 2003, 213(2): 135−150.

还原氧化石墨烯负载氧化钴杂化纳米催化剂的合成及其对一氧化碳氧化的催化性能

王 燕[1,4]，陈泽华[2]，黄 静[3]，李高杰[2]，曹建亮[2]，张 波[2]，陈兴颖[2]，张火利[2]，贾 磊[2]

1. 河南理工大学 安全科学与工程学院，焦作 454003；
2. 河南理工大学 化学化工学院，焦作 454003；
3. 中国石油化工股份有限公司 石油工程技术研究院，北京 100101；
4. 煤炭安全生产河南省协同创新中心，焦作 454003

摘 要：采用沉淀和水热合成方法制备还原氧化石墨烯负载氧化钴纳米催化剂。采用 XRD、Raman 光源、SEM、TEM、氮气吸附、UV−Vis、XPS 和 H_2-TPR 等测试手段对所合成的催化剂进行表征。结果表明：颗粒尺寸均一的钴氧化物纳米颗粒均匀地分散在还原氧化石墨烯表面，所合成的材料具有较大的比表面积和均一的孔径分布。采用连续流动固定床微反−色谱装置对所合成的杂化催化剂对一氧化碳氧化的催化性能进行研究后发现，含还原氧化石墨烯质量分数为 30%的催化剂具有最高的催化活性，能实现一氧化碳在 100 °C 时的完全氧化。

关键词：还原氧化石墨烯；氧化钴；催化剂；一氧化碳氧化；催化性能

(Edited by Wei-ping CHEN)